Hindawi
Advances in Materials Science and Engineering
Volume 2019, Article ID 6753658, 14 pages
https://doi.org/10.1155/2019/6753658

Research Article

Sustainable Development of Corrosion Inhibitors from Electronic Scrap: Synthesis and Electrochemical Performance

J. Porcayo-Calderon,[1] **J.J. Ramos-Hernandez**,[2] **E. Porcayo-Palafox**,[1] **L.M. Martínez de la Escalera**,[3] **J. Canto**,[3] **J.G. Gonzalez-Rodriguez**,[1] **and L. Martinez-Gomez**[2,3]

[1]*CIICAp, Universidad Autónoma del Estado de Morelos, Avenida Universidad 1001, 62209 Cuernavaca, Mor, Mexico*
[2]*Instituto de Ciencias Físicas, Universidad Nacional Autónoma de México, Avenida Universidad s/n, 62210 Cuernavaca, Mor, Mexico*
[3]*Corrosion y Protección (CyP), Buffon 46, 11590 México City, Mexico*

Correspondence should be addressed to J. Porcayo-Calderon; jporcayoc@gmail.com

Received 29 January 2019; Revised 8 August 2019; Accepted 19 November 2019; Published 6 December 2019

Academic Editor: Mikhail Zheludkevich

Due to its high content of rare earths, the use of permanent magnets can be a sustainable alternative for the synthesis of environmentally friendly corrosion inhibitors in order to replace the use of highly toxic inhibitors, as well as the use of rare earth salts of high purity and high cost. In this study, the recovery of rare earths from permanent magnet wastes and their synthesis to chloride salts were carried out. Rare earth chlorides were evaluated as corrosion inhibitors by electrochemical techniques on API X70 steel in a 3.5% NaCl solution. Both anodic and cathodic polarization curves were made, and measurements of both open-circuit potential, linear polarization resistance, and electrochemical impedance were made. Results show that the inhibitor synthesized is a mixture of Nd and Pr chloride. Its performance as a corrosion inhibitor is superior to that of high purity Nd chloride (analytical reagent). The results show that the use of electronic scrap is a sustainable source for the synthesis of green corrosion inhibitors with low carbon footprint.

1. Introduction

Due to the great technological advances of the last decades, today there is a great demand for highly specific materials for the manufacture of high technology equipment. This has created a big problem due to the depletion of raw primary minerals which are nonrenewable resources. At the end of their useful life, they become waste with a high content of valuable strategic metals as well as potential environmental contaminants. For this reason, the correct disposal of electronic waste can contribute to satisfy part of the demand for strategic metals, the recovery of valuable metals, and the protection of the environment. In general, electronic waste can contain up to 60% of metals; however, its use is limited mainly due to high labor costs and strict environmental regulations in certain countries. For this reason, many of these electronic wastes end up in underdeveloped countries for their possible exploitation due to the low cost of labor or in sanitary landfills due to the absence of strict environmental regulations. Raw electronic waste may contain a higher strategic metal content than that found in primary raw minerals. This has motivated the exploitation of the so-called urban mining in order to recover several metals found in electronic scrap [1–3].

Only permanent magnets are a type of electronic waste that has a content of strategic metals much higher than that found in raw primary minerals. This kind of electronic waste can be subjected to a direct recycling process (new magnets) or indirect recycling (recovery of rare earths). Rare earths are considered strategic metals, and their recovery can contribute to satisfy their global demand. Although rare earths in terms of abundance are not rare, in geographical terms,

their production is concentrated in a few countries where their extraction and purification processes have been criticized for the environmental impacts generated. From the permanent magnets, it is possible to recover Nd and other rare earths in smaller content (Pr, Dy, and Ce) [4–6].

Because neodymium is a critical element for the development of new sustainable technologies, there is much interest in the development of technologies that allow its recovery from electronic scrap [2, 4, 6–16]. On the other hand, in the field of corrosion, many studies have also been cited about the corrosion-inhibiting capabilities of rare earth-based compounds. Its use has been proposed as an alternative to replace those inhibitors that are toxic for both people and the environment. However, despite the fact that most studies have focused on compounds based on Ce and La [17–23], the use of neodymium salts can also be an alternative to mitigate the corrosion problems. In a recent study, the authors have reported that neodymium chloride has excellent corrosion inhibition efficiency for API X70 steel immersed in a chloride-rich solution [24].

However, a common factor of these studies is that the rare earth salts evaluated as corrosion inhibitors are of high purity and therefore their cost can be high. Therefore, this study proposes the sustainable use of electronic scrap based on permanent magnets for the synthesis of corrosion inhibitors friendly to the environment and due to its origin with low carbon footprint. The study carried out includes the recovery of rare earths from permanent magnet scrap, their synthesis to rare earth chlorides, and their performance evaluation as an inhibitor of corrosion on API X70 steel by means of electrochemical techniques in a saline solution.

2. Experimental Procedure

2.1. Processing of Permanent Magnets. Chemical composition of the permanent magnets is mainly Fe-Nd-B; however, many of them also contain other rare earths in smaller quantities, being mainly Pr and Dy. In general, its elemental chemical composition can vary between 20 and 40 wt.% of rare earth metals, 60–70 wt.% iron with ~1 wt.% of boron. In the literature, a large number of processes for the recovery of rare earths from permanent magnets are reported [2, 4, 6–16]. In this study, the extraction process of rare earths for their use in the synthesis of corrosion inhibitors was carried out according to what is indicated in Figure 1.

In summary, the permanent magnets were demagnetized by means of heat treatment at 300°C for 2 hours. Subsequently, they were crushed in a hammer mill to a particle size of 0.5 mm on average. An amount of 100 grams of permanent magnet grit was subjected to an acid digestion process in 400 ml of HCl (36% v/v) at room temperature until completely digested, in order to obtain a solution of metal chlorides:

$$\begin{aligned} 2RE + 6HCl &\longrightarrow 2RECl_3 + 3H_2\uparrow \\ Fe + 2HCl &\longrightarrow FeCl_2 + H_2\uparrow \end{aligned} \quad (1)$$

Because the Fe-Nd-B alloy dissolves rapidly in hydrochloric acid, it is necessary to remove by filtration the supernatant of Ni flakes corresponding to the metallic coating of the magnets. Subsequently, the selective precipitation of the rare earths is carried out by adding 250 ml of a 15% oxalic acid solution (wt.%) at room temperature, in order to obtain a white precipitate:

$$2RECl_3 + 3H_2C_2O_4 \longrightarrow RE_2(C_2O_4)_3 + 6HCl \quad (2)$$

The rare earth oxalate precipitate is separated by filtration. In order to eliminate the possible surface contamination of the precipitated oxalates, they are subjected to a washing process with a diluted solution of HCl (5% v/v) for one minute, and then they are subjected to two stages of washing with hot water (50°C) for 10 minutes each. The rare earth oxalates are dried and then subjected to a calcination process at 900°C for 10 hours for conversion to rare earth oxides. The product obtained will be 30 to 50 grams depending on the rare earth content of the initial mixture of permanent magnets.

Figure 1: Recovery of rare earths from scrap of permanent magnets.

2.2. Synthesis of Corrosion Inhibitor. The synthesis of the corrosion inhibitors was made from the rare earth oxides obtained from the permanent magnets. To do this, the oxides were dissolved in a dilute solution of HCl (25% v/v) with constant stirring at room temperature until a clear solution was obtained. The solution of rare earth chlorides was brought to dryness at 60°C until obtaining the corresponding rare earth chlorides:

$$RE_2O_3 + 6HCl \longrightarrow 2RECl_3 + 3H_2O \xrightarrow{\Delta} 2RECl_3 \cdot 6H_2O \quad (3)$$

2.3. Electrochemical Evaluation. In order to compare the performance of the inhibitor synthesized from permanent magnets, its electrochemical evaluation was carried out in the same way as described by the authors in a previous work where neodymium chloride (analytical reagent, AR) was used as a corrosion inhibitor [24].

In short, API X70 steel was used as the working electrode (reaction area = 1 cm^2). The encapsulated samples of API X70 steel were mirror polished with 0.5 micron diamond paste. The corrosive medium was a 3.5% sodium chloride solution (200 ml), and the inhibition efficiency was determined as a function of the added inhibitor concentration, namely, 0.0001 M, 0.0005 M, 0.001 M, 0.005 M, and 0.01 M. Molar concentrations were calculated considering an average molecular weight based on the concentration of Nd and Pr (see Section 3.1). Its evaluation was carried out in an electrochemical cell with 3 electrodes, the API X70 steel being the working electrode, the reference electrode one of saturated calomel (SCE), and a graphite bar as a counter

electrode. Electrochemical measurements performed included polarization curves (the anodic and cathodic branch were performed separately) and measurements of open-circuit potential (OCP), linear polarization resistance (LPR), and electrochemical impedance spectroscopy (EIS). With respect to depolarization curves, the cathodic branch was obtained by polarizing the working electrode from 30 mV up to −400 mV with respect to the OCP value and the anodic branch from −30 mV up to 500 mV with respect to the OCP value, both at a scanning rate of 10 mV/min and after 24 hours of immersion of the working electrode in the electrolyte (with and without inhibitor). The OCP and LPR measurements were performed at one-hour intervals during the first 24 hours and then every 3 hours. LPR measurements were performed at a scanning rate of 10 mV/min and ±10 mV with respect to its open-circuit potential. EIS measurements were performed with a perturbation of ±10 mV and frequency range from 100 kHz to 0.01 Hz. Potentiodynamic polarization curves were performed in a Gill AC potentiostat/galvanostat from ACM Instruments and the OCP, LPR, and EIS measurements in an Interface 1000 potentiostat/galvanostat from Gamry. All electrochemical measurements were performed at room temperature and in triplicate.

2.4. Complementary Analysis. The reported X-ray diffraction analyses were performed on a Bruker© diffractometer model D8 Advance that uses Cu-Kα_1 radiation. The wavelength used to collect the intensity data was 1.5406 angstroms. The acceleration voltage and the current density used were 40 kV and 25 mA, respectively. The measurements were made in a range of 2θ from 10° to 100° with a step of 0.0203° with a residence time of 0.2 seconds.

Electron microscopic analyses were performed on a JEOL JSM-IT500 scanning electron microscope (SEM) equipped with a Bruker-XFlash 6|30 energy dispersive spectrometry (EDS) detector. Both element mappings and EDS spectra were obtained with an acceleration voltage of at least 20 kV.

3. Results and Discussion

3.1. Inhibitor Characterization. For comparison purposes, Figure 2 shows the morphological aspect of neodymium oxide (AR) and the oxide of rare earths obtained through the hydrometallurgical process of the permanent magnets. It can be observed that the neodymium oxide (AR) is formed by micrometric particles of different sizes, and an approach to one of them allows us to observe that each particle is composed of agglomerates of sub-micrometric particles. In the case of rare earth oxides recovered from permanent magnets, very similar characteristics were observed, mainly with respect to the particles size; however, an approach to one of them allows us to observe that these are formed by the agglomeration of micrometric particles with different shapes (blocks).

Figure 3 shows the element mapping of the rare earth oxide particles recovered from permanent magnets. In general, a homogeneous distribution of both Nd and Pr can be observed. That is, there was no segregation of the oxides.

EDS analysis of the particles (Figure 4) allows observing that their chemical composition corresponds to a mixture of both neodymium and praseodymium oxides, and the element mapping (not shown) indicated that they are homogeneously distributed. The analysis of Nd and Pr indicated a Nd content of 87–88% (wt.%) and the rest of Pr. Because Nd and Pr have similar properties, their separation is difficult and therefore the presence of Pr is common in permanent magnets [6].

X-ray diffraction characterization of both oxides is shown in Figure 5. According to the spectra, it can be observed that the rare earth oxides recovered from permanent magnets are really a mixture of Nd_2O_3, Pr_2O_3, and a majority phase possibly of a solid solution of $Pr_{2-x}Nd_xO_3$. It was not possible to find in the database the file corresponding to the solid solution. In addition, unfortunately, the literature on the recycling of rare earths from permanent magnets does not report the morphological and structural characterization of the oxides obtained, making it difficult for the authors to make a more detailed analysis. However, according to studies reported on the synthesis of oxides from the La-Nd-O-C system [25], it is possible to infer that the majority phase is a complex oxide of the form $Pr_{2-x}Nd_xO_3$. This assumption is based on the similarity of the studies reported, where the authors studied a mixture of La and Nd citrates, and in the case of the present study, a mixture of Nd and Pr oxalates was used. In both cases, the anions act as chelating agents for rare earth cations.

Figure 6 shows the X-ray diffractograms of the rare earth (RE) chlorides synthesized from permanent magnets. The identification showed the presence of a mixture of both neodymium and praseodymium chlorides in a proportion close to 90 : 10 according to the metallic content of rare earth previously determined.

3.2. Potentiodynamic Polarization Curves. Figures 7 and 8 show the anodic and cathodic branches of API X70 steel in 3.5% NaCl solution with the addition of inhibitor at different concentrations and room temperature. Both graphs show that with the inhibitor addition, there is a displacement of the potential towards more active values (except at the lowest concentration), as well as a displacement of both curves towards lower current densities. From the anodic branch, it is observed that the inhibitor addition caused an increase in its slope at potentials above the corrosion potential; in addition, the position of the cathodic branches indicates that the inhibitor addition causes its displacement towards lower current densities. The greatest displacement was obtained with the addition of inhibitor at concentrations of 0.0005 and 0.001 M, and at higher concentrations, the displacement tends to decrease.

Table 1 shows the electrochemical parameters of the anodic and cathodic polarization curves. According to the values of the electrochemical parameters, it is observed that due to the displacement of the polarization curves at lower current densities, both the anodic and cathodic slopes tend

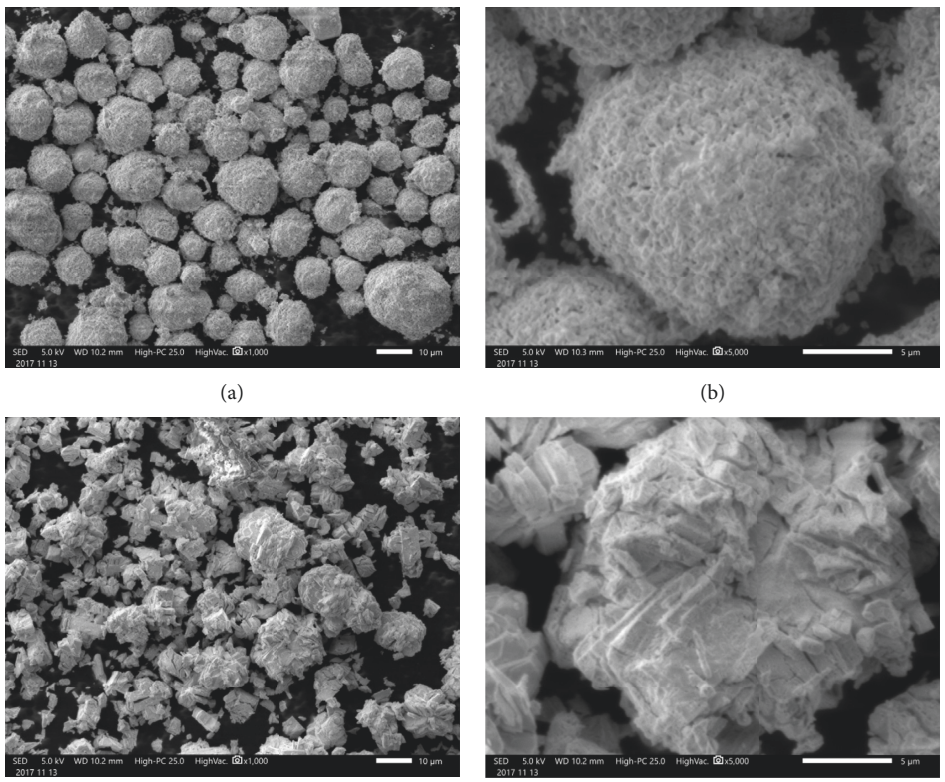

Figure 2: Morphological aspects of rare earth oxides: (a, b) Nd_2O_3 (AR) and (c, d) rare earth oxides recovered from permanent magnets.

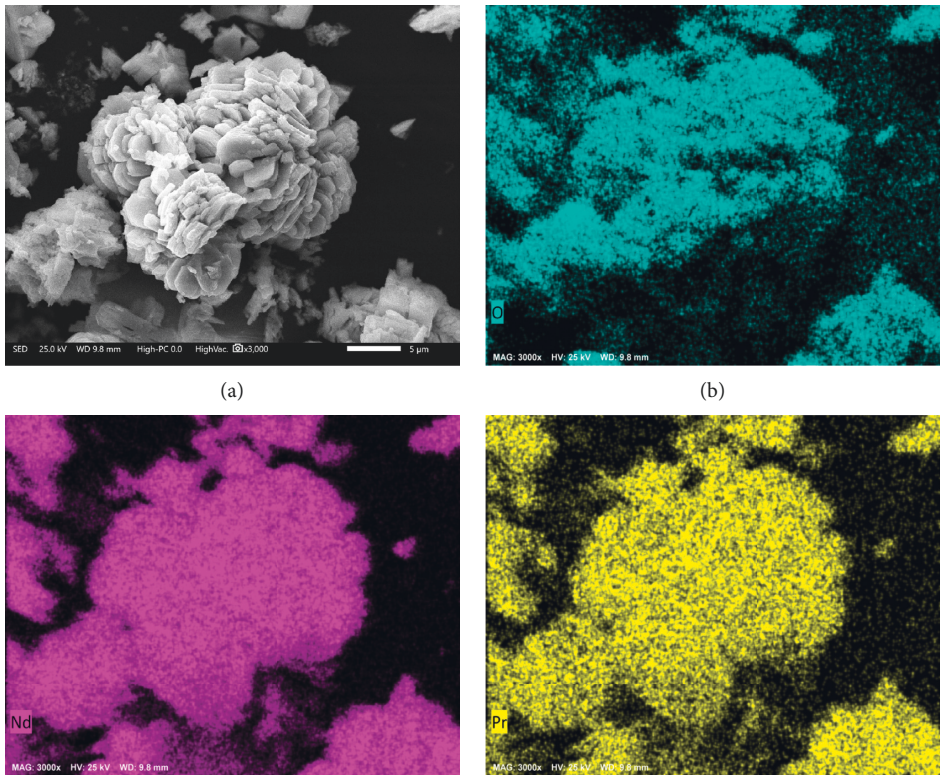

Figure 3: Element mapping of the rare earth oxides recovered from permanent magnets.

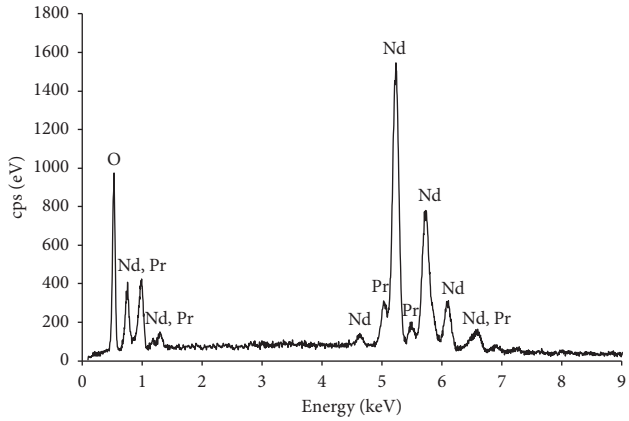

Figure 4: EDS spectrum of the rare earth oxides from permanent magnets.

to decrease; this effect is more visible in the values of the cathodic slopes. The corrosion current density values, both anodic and cathodic, decrease when increasing the concentration of inhibitor up to 0.001 M; higher concentrations cause a slight increase in their values. This increase can be associated with the increase in the concentration of Cl^- ions due to the high concentration of added inhibitor [20]. The decrease in both the cathodic slope as well as the cathodic corrosion current density shows that the presence of the inhibitor affected the oxygen reduction reaction [21, 24], as a consequence of the precipitation of the lanthanide ions (oxides and/or hydroxides) onto cathodic sites present on the steel surface [18–21, 24, 26, 27]. On the other hand, similarly, the decrease of both the anodic slope and the anodic corrosion current density shows that the inhibitor also affects the metal dissolution reaction, possibly due to the formation or precipitation of a protective film on the surface metallic. These changes suggest that the inhibitor acts as a mixed inhibitor [18–20, 24]. The changes observed in the polarization curves, as well as in the magnitude of the electrochemical parameters, indicate that the performance of the inhibitor based on permanent magnets is similar to that observed with neodymium chloride (AR) according to the authors' previous work [24].

3.3. Open-Circuit Potential (OCP) Measurements. Figure 9 shows the evolution of OCP values for API X70 steel at different concentrations of inhibitor in 3.5% NaCl solution at room temperature. In all cases, an abrupt drop in the OCP values is observed up to 10 hours of immersion, and later, the changes tend to be more stable. In the inhibitor's absence, the steel showed the most active OCP values, and in the presence of the inhibitor, the noblest OCP values are observed. At inhibitor concentrations greater than 0.0001 M, it is observed that the OCP values tend to be the same value after 50 hours of immersion. Some authors [18, 19] consider that the abrupt drop in OCP values, at the beginning of the test, is associated with the reorganization of the corrosion products' layers. However, although in the presence of the inhibitor there is an effect in the oxygen reduction reaction and a displacement of the OCP values in the noble direction, these changes do not define it as an anodic or cathodic type inhibitor, but rather as a mixed type inhibitor [28, 29]. Again, the observed behavior is very similar to that obtained with neodymium chloride (AR) [24].

3.4. Linear Polarization Resistance Measurements. Figure 10 shows the evolution of the polarization resistance values for API X70 steel at different concentrations of inhibitor. In the absence of inhibitor, it is observed that at the beginning of the test, the steel presented variations in its polarization resistance values, and after 20 hours of immersion, they remained almost constant. This indicates an active corrosion process at the beginning of the test, and subsequently, the accumulation of corrosion products decreased the exposed metal area and/or the diffusion rate of the aggressive electrolyte ions. However, with the inhibitor addition, at all concentrations, a rapid increase in the resistance values was observed in the first 10 hours of immersion. The smallest increase was observed with both the lowest and the highest concentration of inhibitor. On the one hand, this may be due to the low concentration of RE cations that are insufficient to block all the cathodic sites, and on the other hand, the increase in the concentration of Cl^- ions increases the corrosivity of the electrolyte. The greatest increase in resistance values was obtained with the addition of inhibitor at a concentration of 0.001 M.

Based on the polarization resistance values, the inhibition efficiency was calculated taking into account the average of the resistance values of the last 50 test hours. Based on these averaged values, Figure 11 shows the inhibition efficiency as a function of inhibitor concentration. It is observed that the inhibition efficiency increases up to a concentration of 0.001 M, and at higher concentrations, it tends to decrease. The efficiency values obtained are greater than 90% and higher than those reported when neodymium chloride (AR) is used as an inhibitor of corrosion [24]. The observed increase in the inhibition efficiency using rare earth chlorides synthesized from permanent magnets was 7%.

3.5. Electrochemical Impedance Spectroscopy Measurements. Figure 12 shows the Nyquist and Bode diagrams for API X70 steel in 3.5% NaCl solution with the addition of the inhibitor synthesized from permanent magnets at different concentrations after 100 hours of immersion. In the absence of the inhibitor, the steel shows the formation of a capacitive semicircle with a diameter less than 1000 $\Omega \cdot cm^2$. The above is consistent with the maximum impedance module value ($<1000\ \Omega \cdot cm^2$) and the presence of a single time constant observed around 10 Hz (maximum phase angle $\approx 54^\circ$).

On the other hand, with the addition of inhibitor, the formation of three time constants is observed. The first constant is observed in the high-frequency region (>1000 Hz), the second one in the intermediate frequency region (>1 Hz, <1000 Hz), and the third one at low frequencies (<1 Hz). The capacitive semicircles have a diameter greater than that observed in the absence of inhibitor, and the increase in diameter indicates a greater charge transfer

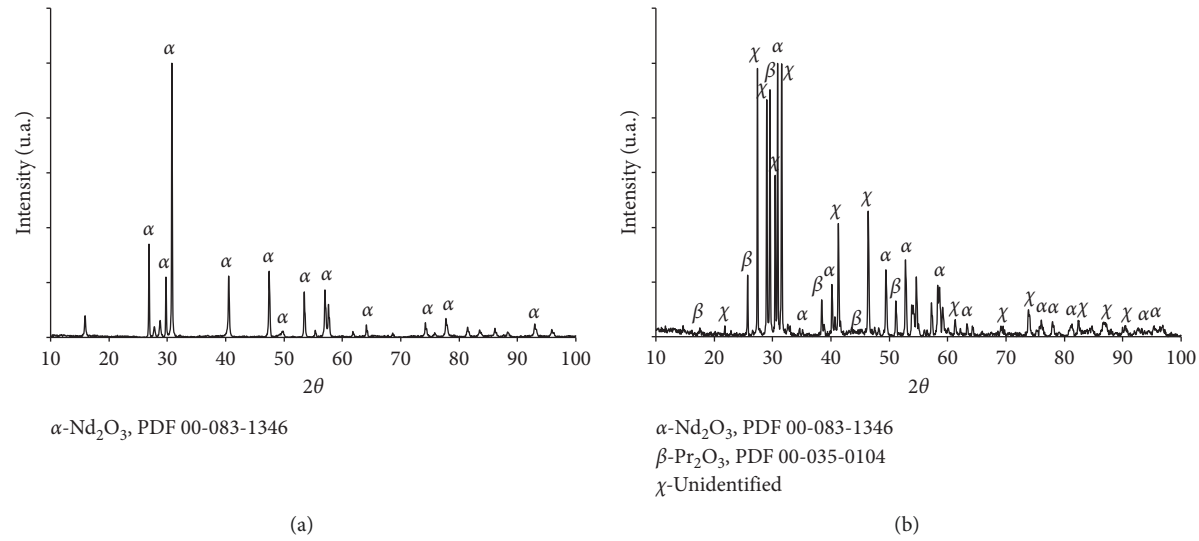

Figure 5: X-ray diffractograms: (a) Nd_2O_3 (AR); (b) rare earth oxides from permanent magnets.

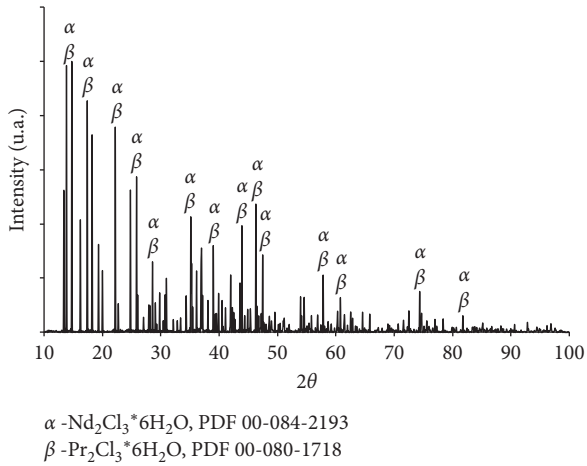

Figure 6: X-ray diffractogram of rare earth chlorides from permanent magnets.

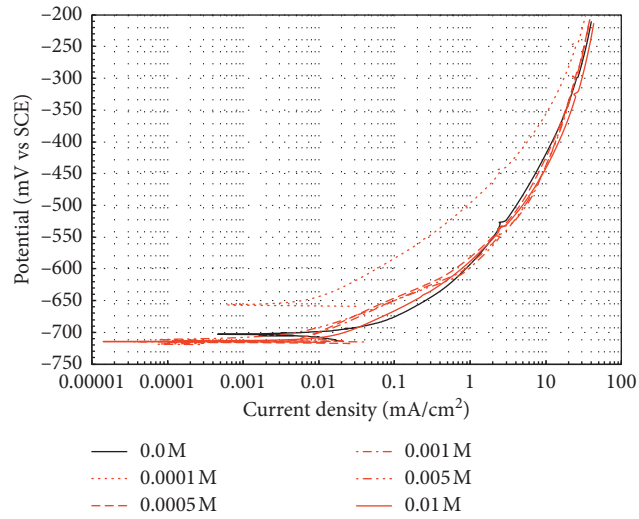

Figure 7: Anodic polarization curves for API X70 steel in 3.5% NaCl solution at different concentrations of inhibitor obtained from permanent magnets.

resistance. Semicircles' diameter increases when increasing the inhibitor concentration up to a concentration of 0.001 M, and at higher concentrations, the diameter tends to decrease. Same trend is observed in the maximum value of the impedance module.

For simplicity, only the evolution of the impedance spectra is presented for the case of inhibitor absence and with the addition of inhibitor at a concentration of 0.001 M (Figures 13 and 14, respectively). Figure 13 shows the evolution of the impedance spectra for API X70 steel in the absence of the inhibitor. From the Nyquist diagram, a trend similar to that observed in the polarization resistance measurements is observed; that is, at the beginning of the test, oscillations are presented in the diameter of the capacitive semicircle, and later, this presents slight variations. The presence of a single capacitive semicircle is congruent with the Bode diagram, in which the presence of a single time constant is observed with a phase angle close to 60° at the beginning of the test, and subsequently, it decreases slightly around 54°; also, it does not show any displacement. Both analyses are congruent with the evolution of the impedance module, $|Z|$, its slope in the intermediate frequency region does not present variations, and in the low frequency region, its values vary according to the diameter variations of the capacitive semicircle.

The characteristics described above are congruent for materials that are not capable of forming a protective oxide (decrease of the phase angle) or that their corrosion products do not have a barrier affect that decreases the diffusion of the aggressive electrolyte ions (a single time constant, not significant variation in the diameter of the capacitive semicircle). The analysis of the steel surface (Figure 15(a)) showed that it was not able to develop a protective oxide on

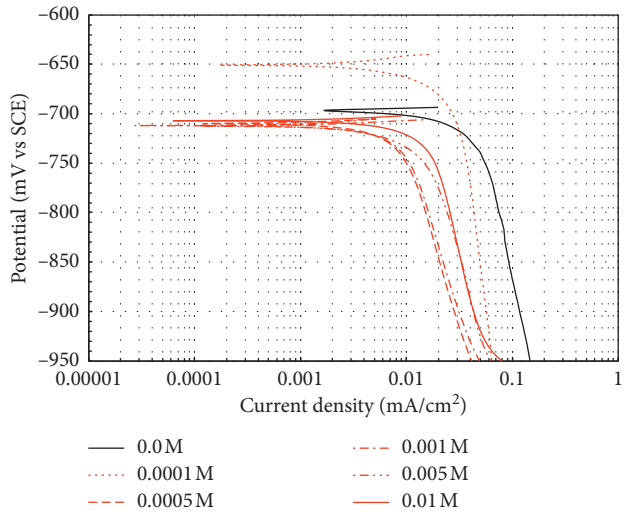

Figure 8: Cathodic polarization curves for API X70 steel in 3.5% NaCl solution at different concentrations of inhibitor obtained from permanent magnets.

Table 1: Electrochemical parameters and standard deviation of the polarization curves as a function of the inhibitor concentration obtained from permanent magnets.

Molar concentration	E_{corr} (mV)	B_a (mv/Dec)	B_c (mV/Dec)	I_{corr} (mA/cm^2)
0.0	−699.38 ± 4.66	72.14 ± 8.30	517.37 ± 10.60	0.046552 ± 0.00139
0.0001	−654.5 ± 2.31	71.85 ± 5.34	665.59 ± 16.72	0.014879 ± 0.01168
0.0005	−712.2 ± 3.60	52.96 ± 4.89	370.47 ± 12.34	0.007367 ± 0.00113
0.001	−713.8 ± 2.79	53.07 ± 3.78	356.25 ± 15.82	0.006708 ± 0.00113
0.005	−712.6 ± 1.74	55.43 ± 2.98	366.51 ± 13.45	0.009949 ± 0.00229
0.01	−712.9 ± 5.26	66.32 ± 4.01	448.78 ± 12.79	0.013163 ± 0.00151

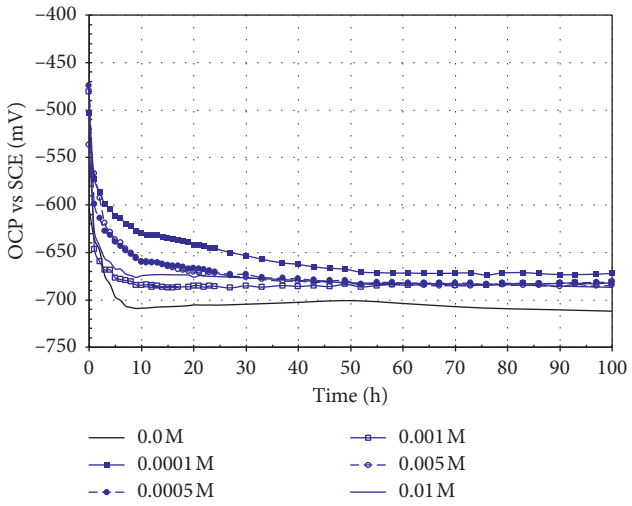

Figure 9: OCP values for API X70 steel in 3.5% NaCl solution at different concentrations of the inhibitor synthesized from permanent magnets.

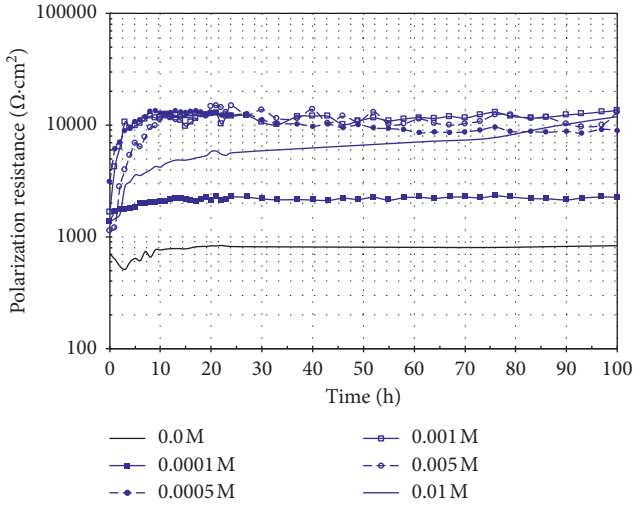

Figure 10: Evolution in polarization resistance values for API X70 steel in 3.5% NaCl solution at different concentrations of inhibitor at room temperature.

its surface; besides, the absence of corrosion products indicates that they were easily detached from the surface. This resulted in a nonuniform corrosion process with pitting attack.

In this case, the fitting of the impedance spectra can be carried out with a simple equivalent circuit like the one shown in Figure 16(a); in this equivalent circuit, the constant phase element (CPE) has been used in order to compensate

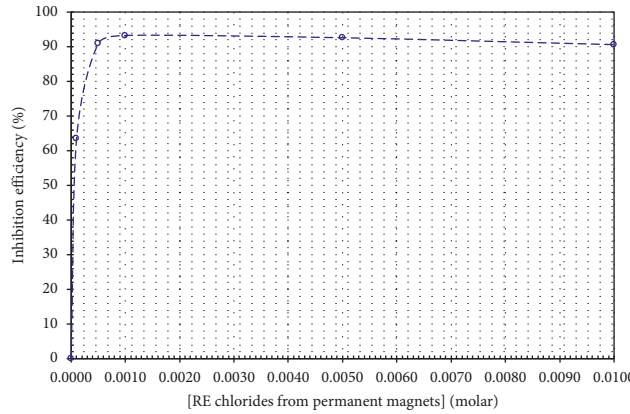

Figure 11: Effect of inhibitor concentration, synthesized from permanent magnets, on the corrosion inhibition efficiency of API X70 steel in 3.5% NaCl solution at room temperature.

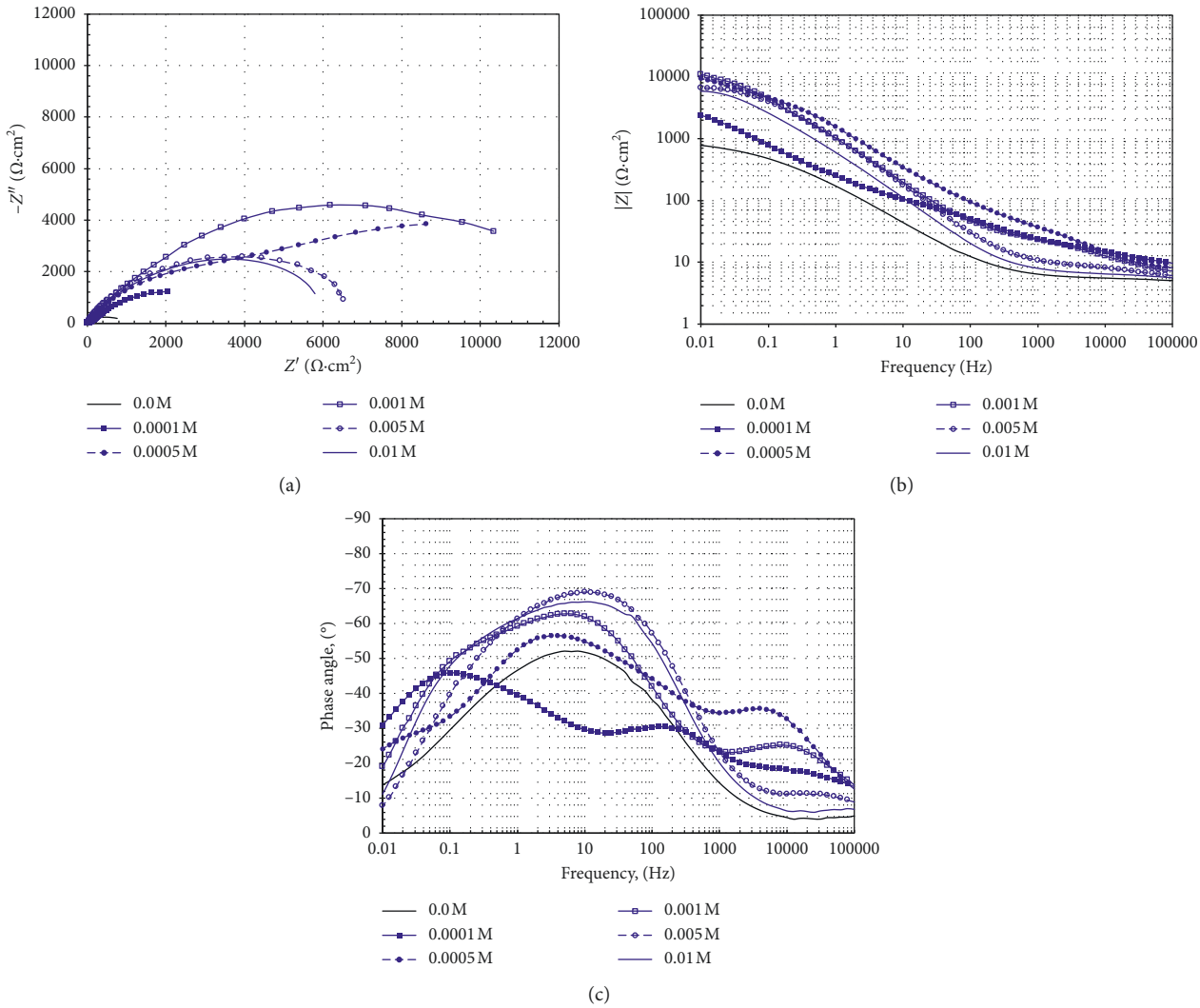

Figure 12: Nyquist and Bode diagrams for API X70 steel with and without the addition of the inhibitor synthesized from permanent magnets at different concentrations after 100 hours immersion in 3.5% NaCl solution at room temperature.

the heterogeneity of the surface of the working electrode, R_s is the electrolyte resistance, R_{ct} is the charge transfer resistance, and Z_{CPEdl} is the impedance of the double layer capacitance. Table 2 shows the evolution of the electrochemical parameters of the impedance spectra. It can mainly be observed that the evolution of the R_{ct} values is similar to

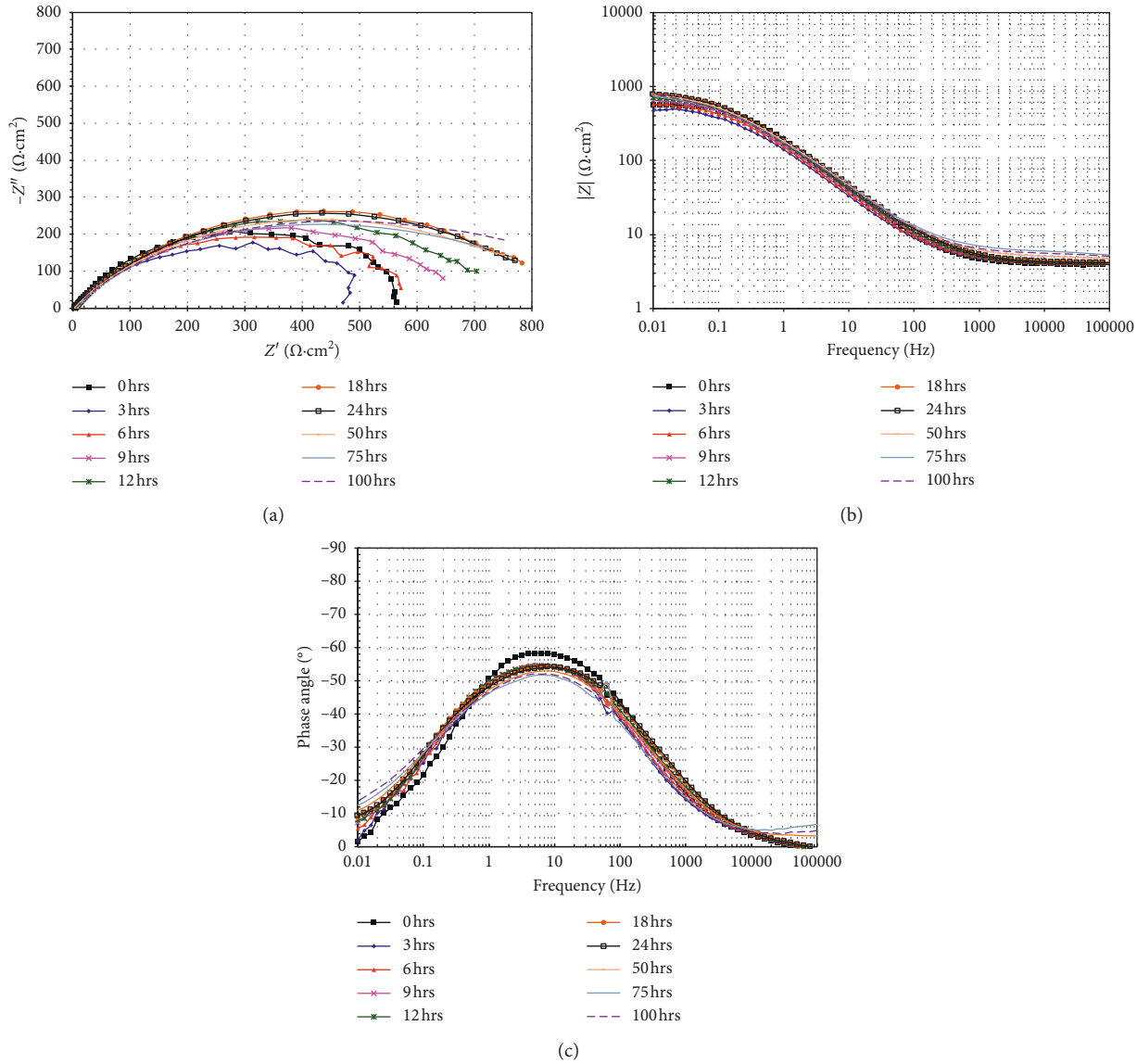

Figure 13: Evolution of Nyquist and Bode diagrams for API X70 steel in 3.5% NaCl solution without inhibitor addition.

the evolution of the polarization resistance values shown in Figure 10; in addition, the constant decrease in the n_{ct} values indicates a loss of the capacitive properties of the steel surface and therefore more susceptible to corrosion.

Analysis of the impedance spectra with the addition of 0.001 M of inhibitor synthesized from permanent magnets (Figure 14) shows the evolution of three time constants which can be located in the three different frequency regions. These time constants are not visible in the Nyquist diagram because the first two constants evolve from the high frequency region to the intermediate frequency region. This is very common in corrosion processes where organic inhibitors adsorb onto the metal surface forming protective films [30–32]; in the Nyquist diagrams, only about 30% of the collected data is visible, and generally, 30% corresponds to data from the low frequency region. In the high-frequency region, the formation and evolution of the first time constant around 10,000 Hz with a maximum phase angle of approximately 25° is observed. The second time constant is observed at 3 hours of immersion in the intermediate frequency region, and it shifts from 30 Hz to 5 Hz reaching a maximum phase angle close to 65°. The third time constant shifts from the intermediate frequency region (time = 0 hours) to the low-frequency region (time > 0 hours), and its maximum phase angle tends to decrease with the immersion time from 60° to 50° approximately. These three time constants are also visible in the evolution of the impedance module spectra. Each of them is associated with the slope changes of the relation $\log f$ vs $\log |Z|$, in the three regions of the frequency.

The formation and evolution of the first two time constants can be related to the typical mechanism of precipitation of hydroxides and oxides for corrosion process inhibited by the addition of compounds based on rare earths [21, 33–36]. In general, the formation of the protective films is due to the hydrolysis reactions of the lanthanide cations

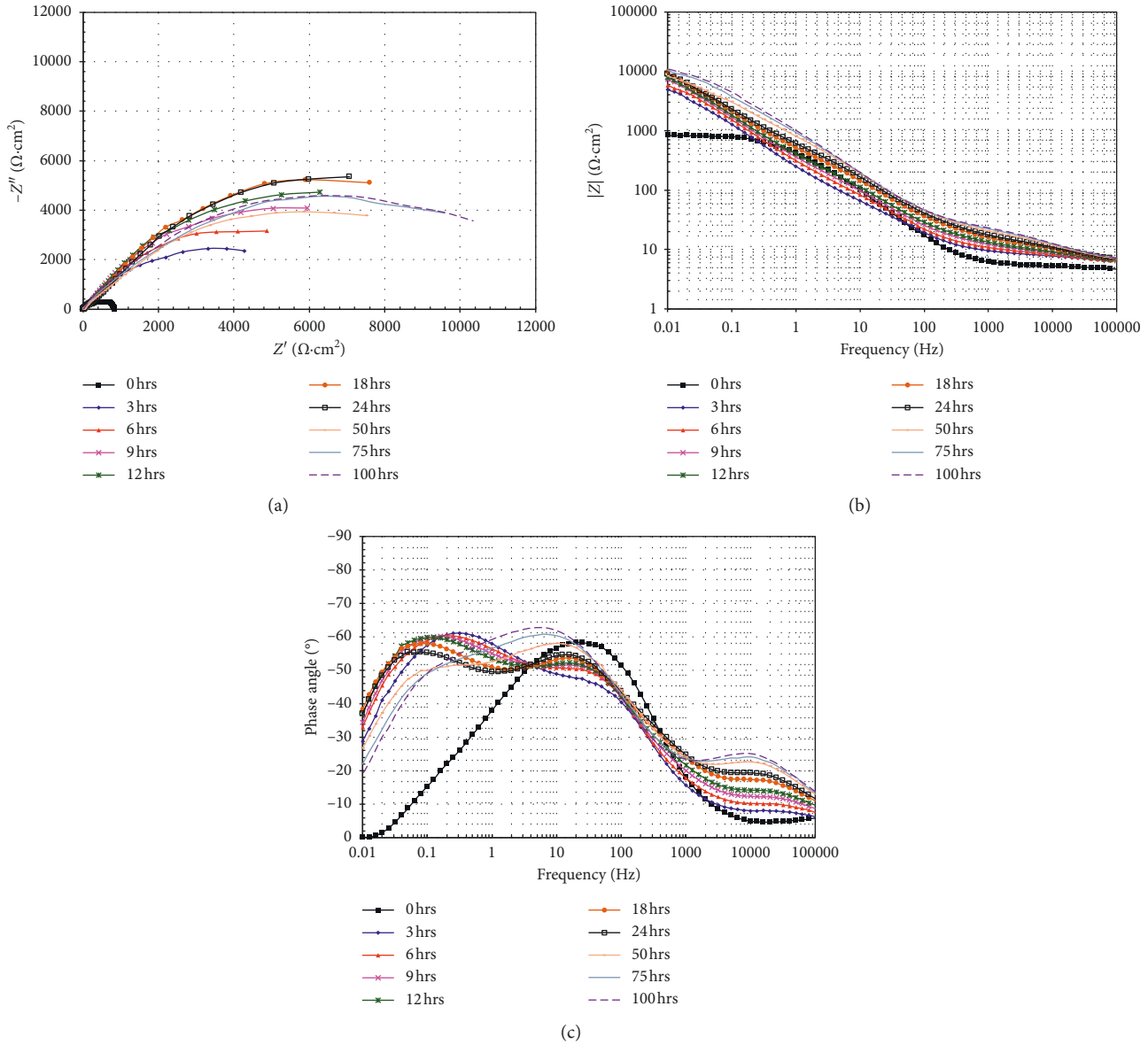

Figure 14: Evolution of Nyquist and Bode diagrams for API X70 steel in 3.5% NaCl solution with the addition of 0.001 M of inhibitor synthesized from permanent magnets.

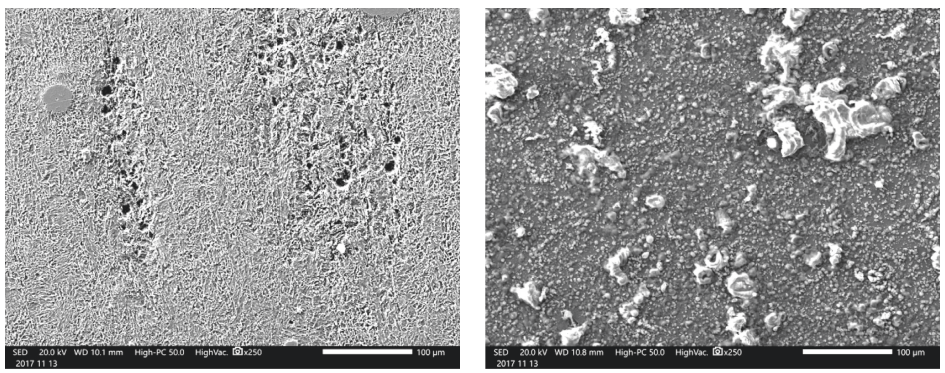

Figure 15: Morphological aspects of the surface of API X70 steel after 100 hours of immersion in a 3.5% NaCl solution at room temperature: (a) without inhibitor; (b) with 0.001 M of inhibitor synthesized from permanent magnets.

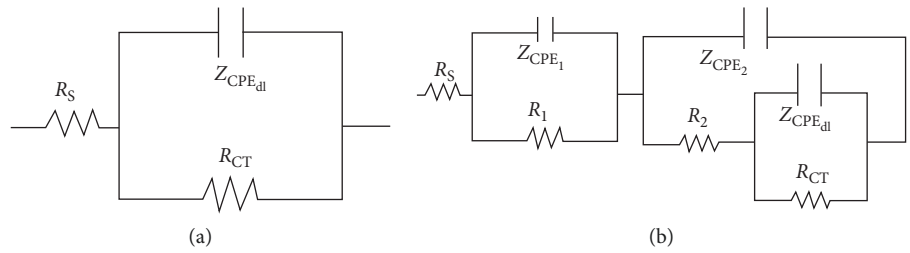

Figure 16: Equivalent circuits: (a) without addition of inhibitor: (b) with addition of inhibitor synthesized from permanent magnets.

Table 2: Evolution of the electrochemical parameters of the EIS spectra of API X70 steel in the absence of inhibitor.

Time (hours)	R_s ($\Omega\cdot cm^2$)	R_{ct} ($\Omega\cdot cm^2$)	Yo_{dl} ($\Omega^{-1}\cdot cm^{-2}\cdot s^n$)	n_{ct}
0	4.0	609	$1.16E-3$	0.73
3	4.1	541	$1.74E-3$	0.70
6	4.1	626	$1.62E-3$	0.69
9	4.1	709	$1.55E-3$	0.68
12	4.1	780	$1.46E-3$	0.68
18	4.1	876	$1.36E-3$	0.68
24	4.1	860	$1.35E-3$	0.67
50	4.8	839	$1.45E-3$	0.66
75	5.5	820	$1.58E-3$	0.65
100	5.2	848	$1.63E-3$	0.65

with the OH^- ions generated at the cathodic sites. Firstly, the precipitation of lanthanide hydroxides, $Ln(OH)_3$, is carried out, and later, they are transformed into more stable lanthanide oxides, Ln_2O_3. The displacement and evolution of the third time constant is due to the formation and evolution of the first two time constants. That is, the precipitation of the rare earth hydroxides forms a new interface with the electrolyte, and its subsequent conversion to protective oxide then also forms another interface (metal-oxide-hydroxide-electrolyte).

Figure 15(b) shows the surface appearance of the steel after 100 hours of testing; on its surface, the presence of a protective layer with visible protuberances is observed. The surface appearance is completely different from that observed in the absence of inhibitor (Figure 15(a)). An approach to the surface (Figure 17) allows us to observe the presence of multiple crystals on the possible cathodic sites of the steel surface. EDS analysis of the metallic surface (EDS spectrum "a") mainly shows the presence of steel elements and a small amount of Nd and Pr; this suggests that initially, the rare earths are adsorbed to the metallic surface possibly as hydroxides. Subsequently, the generation of OH^- ions, in the cathode sites, favors their conversion to oxides ($2Ln(OH)_3 = Ln_2O_3 + 3H_2O$) forming small crystals (EDS spectrum "b"). The growth of these crystals forms rose-like formations (EDS spectrum "c") with a similar shape to the crystals called "desert rose." Subsequently, these structures coalesce, forming a protective layer of rare earth oxyhydroxides (EDS spectrum "d"). Again, the morphological aspects of the formed surface layers are identical to those observed with the addition of neodymium chloride (AR) [24].

Fitting of the impedance spectra was performed according to the equivalent circuit shown in Figure 16(b). The parameter χ^2 (chi-square) was used as a criterion to fitting the experimental data to the proposed equivalent circuits. Fitting was considered satisfactory if $\chi^2 < 10^{-3}$. This equivalent circuit was used for the impedance spectra obtained from 3 hours; for the initial impedance spectrum (0 hour), its adjustment was made with the equivalent circuit of Figure 16(a). The first time constant associated with the layer of lanthanide hydroxides adsorbed onto metal surface is represented by R_1 and Z_{CPE1}, where R_1 is the resistance and Z_{CPE1} the impedance of the constant phase element. The second time constant associated with the lanthanide oxide layer is represented by R_2 and Z_{CPE2}, where R_2 is the resistance and Z_{CPE2} the impedance of the constant phase element, and the third time constant is associated with R_{ct} and Z_{CPEdl} already defined. Table 3 shows the evolution of the electrochemical parameters of the impedance spectra. According to the obtained values, it is observed that R_1 remains practically constant with low resistance values; this can be congruent for a film adsorbed with low thickness. R_2 shows a constant increase in its values with the immersion time; this is consistent with the formation of a protective film of lanthanide oxides, and the R_{ct} values also tend to increase, and after 9 hours of immersion, their values remain practically constant. On the other hand, the values of n indicate that the formation of the layers of oxides and hydroxides onto surface increased the capacitive properties of the metal surface. In addition, it can be observed that the Yo values are of the same order of magnitude, but of smaller magnitude than those obtained in the absence of inhibitor (Table 2). Since Yo is directly proportional to the capacitance and inversely proportional to the resistance, this indicates a greater corrosion resistance of the metal surface [37]. Based on the resistance values obtained, it can be seen that the sum of them ($R_1 + R_2 + R_{ct}$) coincides with the magnitude and

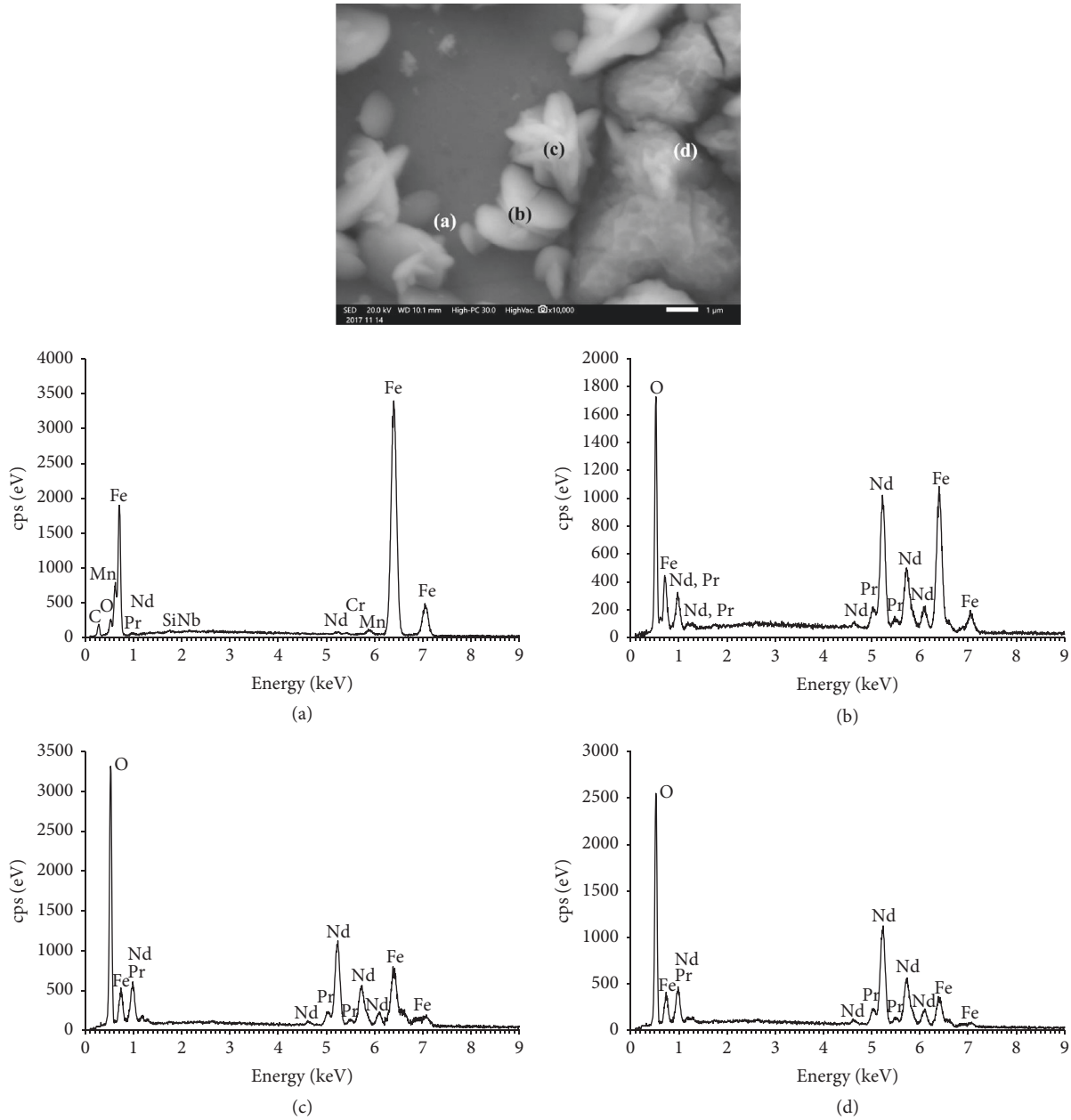

Figure 17: Surface aspect and EDS analysis of the API X70 steel after 100 hours of immersion in 3.5% NaCl solution with the addition of 0.001 M of inhibitor synthesized from permanent magnets.

Table 3: Evolution of electrochemical parameters of the EIS spectra after 100 hours of immersion in 3.5% NaCl solution with 0.001 M of inhibitor synthesized from permanent magnets.

Time (hours)	R_1 ($\Omega\cdot cm^2$)	Yo_1 ($\Omega^{-1}\cdot cm^{-2}\cdot s^n$)	n_1	R_2 ($\Omega\cdot cm^2$)	Yo_2 ($\Omega^{-1}\cdot cm^{-2}\cdot s^n$)	n_2	Rct ($\Omega\cdot cm^2$)	Yo_{dl} ($\Omega^{-1}\cdot cm^{-2}\cdot s^n$)	n_{ct}
0	—	—	—	—	—	—	838	$4.08E-4$	0.78
3	5.50	$2.46E-4$	0.60	146	$5.14E-4$	0.75	6844	$5.33E-4$	0.79
6	5.13	$5.27E-4$	0.52	268	$4.66E-4$	0.75	9557	$4.38E-4$	0.78
9	4.47	$1.48E-3$	0.41	410	$4.24E-4$	0.75	12037	$3.97E-4$	0.80
12	4.67	$9.01E-4$	0.45	576	$4.08E-4$	0.74	11489	$3.66E-4$	0.81
18	5.08	$3.70E-4$	0.53	984	$3.50E-4$	0.73	12191	$3.41E-4$	0.83
24	5.41	$1.84E-4$	0.59	1215	$3.06E-4$	0.74	11315	$3.50E-4$	0.78
50	5.58	$1.07E-4$	0.63	1521	$2.27E-4$	0.76	12631	$2.82E-4$	0.77
75	5.73	$9.22E-4$	0.64	3095	$2.22E-4$	0.78	11124	$2.03E-4$	0.78
100	5.73	$8.90E-4$	0.64	3751	$2.00E-4$	0.79	11662	$1.65E-4$	0.76

tendency of the polarization resistance values shown in Figure 10. All the results shown indicate that the use of electronic scrap (permanent magnets) is a reliable source for the synthesis of rare earth-based corrosion inhibitors.

4. Conclusions

The use of electronic scrap is a viable source for the synthesis of compounds with inhibitory properties of corrosion. The synthesis process of the inhibitors is simple, producing a mixture of neodymium- and praseodymium-based chlorides. The electrochemical studies on the performance of the mixture of chlorides synthesized showed an inhibition efficiency greater than 90%, and the optimal concentration of inhibition was 0.001 M. Its protective action is due to the reduction of the oxygen reduction rate due to a blocking effect of the cathodic sites and to the reduction of the metallic dissolution rate due to the formation of a protective layer based on rare earth oxyhydroxides. Both characteristics define it as a mixed type inhibitor.

Data Availability

The data used to support the findings of this study are available from the corresponding author upon request.

Conflicts of Interest

The authors declare that there are no conflicts of interest regarding the publication of this paper.

Acknowledgments

Financial support from the Consejo Nacional de Ciencia y Tecnología (CONACYT, México) (Project 232611 "Laboratorio Nacional de Materias Primas, Metalurgia y Aleaciones Estratégicas Basadas en Tierras Raras Orientadas a Fortalecer la Sustentabilidad de los Sectores Energía, Transporte y Comunicaciones") is gratefully acknowledged. The authors are grateful for the comments and support provided by M. Casales-Diaz.

References

[1] L. Zhang and Z. Xu, "A review of current progress of recycling technologies for metals from waste electrical and electronic equipment," *Journal of Cleaner Production*, vol. 127, pp. 19–36, 2016.

[2] Z. Sun, Y. Xiao, H. Agterhuis, J. Sietsma, and Y. Yang, "Recycling of metals from urban mines—a strategic evaluation," *Journal of Cleaner Production*, vol. 112, pp. 2977–2987, 2016.

[3] S. Ilyas, J.-C. Lee, and R.-A. Chi, "Bioleaching of metals from electronic scrap and its potential for commercial exploitation," *Hydrometallurgy*, vol. 131-132, pp. 138–143, 2013.

[4] R. Schulze and M. Buchert, "Estimates of global REE recycling potentials from NdFeB magnet material," *Resources, Conservation and Recycling*, vol. 113, pp. 12–27, 2016.

[5] L. A. Diaz, T. E. Lister, J. A. Parkman, and G. G. Clark, "Comprehensive process for the recovery of value and critical materials from electronic waste," *Journal of Cleaner Production*, vol. 125, pp. 236–244, 2016.

[6] B. Sprecher, R. Kleijn, and G. J. Kramer, "Recycling potential of neodymium: the case of computer hard disk drives," *Environmental Science & Technology*, vol. 48, no. 16, pp. 9506–9513, 2014.

[7] G. G. Zaimes, B. J. Hubler, S. Wang, and V. Khanna, "Environmental life cycle perspective on rare earth oxide production," *ACS Sustainable Chemistry & Engineering*, vol. 3, no. 2, pp. 237–244, 2015.

[8] P. Venkatesan, Z. H. I. Sun, J. Sietsma, and Y. Yang, "An environmentally friendly electro-oxidative approach to recover valuable elements from NdFeB magnet waste," *Separation and Purification Technology*, vol. 191, pp. 384–391, 2018.

[9] J. H. Rademaker, R. Kleijn, and Y. Yang, "Recycling as a strategy against rare earth element criticality: a systemic evaluation of the potential yield of NdFeB magnet recycling," *Environmental Science & Technology*, vol. 47, no. 18, pp. 10129–10136, 2013.

[10] Y. Xu, L. S. Chumbley, and F. C. Laabs, "Liquid metal extraction of Nd from NdFeB magnet scrap," *Journal of Materials Research*, vol. 15, no. 11, pp. 2296–2304, 2000.

[11] M. Zakotnik, I. R. Harris, and A. J. Williams, "Possible methods of recycling NdFeB-type sintered magnets using the HD/degassing process," *Journal of Alloys and Compounds*, vol. 450, no. 1-2, pp. 525–531, 2008.

[12] J. P. Rabatho, W. Tongamp, Y. Takasaki, K. Haga, and A. Shibayama, "Recovery of Nd and Dy from rare earth magnetic waste sludge by hydrometallurgical process," *Journal of Material Cycles and Waste Management*, vol. 15, no. 2, pp. 171–178, 2013.

[13] T. Vander Hoogerstraete, B. Blanpain, T. Van Gerven, and K. Binnemans, "From NdFeB magnets towards the rare-earth oxides: a recycling process consuming only oxalic acid," *RSC Advances*, vol. 4, no. 109, pp. 64099–64111, 2014.

[14] M. A. R. Önal, C. R. Borra, M. Guo, B. Blanpain, and T. Van Gerven, "Recycling of NdFeB magnets using sulfation, selective roasting, and water leaching," *Journal of Sustainable Metallurgy*, vol. 1, no. 3, pp. 199–215, 2015.

[15] D. D. München and H. M. Veit, "Neodymium as the main feature of permanent magnets from hard disk drives (HDDs)," *Waste Management*, vol. 61, pp. 372–376, 2017.

[16] M. A. R. Önal, E. Aktan, C. R. Borra, B. Blanpain, T. Van Gerven, and M. Guo, "Recycling of NdFeB magnets using nitration, calcination and water leaching for REE recovery," *Hydrometallurgy*, vol. 167, pp. 115–123, 2017.

[17] H. Allachi, F. Chaouket, and K. Draoui, "Corrosion inhibition of AA6060 aluminium alloy by lanthanide salts in chloride solution," *Journal of Alloys and Compounds*, vol. 475, no. 1, pp. 300–303, 2009.

[18] D. Mohammedi, F. Ismail, R. Rehamnia, R. Bensalem, and O. Savadogo, "Corrosion behaviour of steel in the presence of rare earth salts: synergistic effect," *Corrosion Engineering, Science and Technology*, vol. 50, no. 8, pp. 633–638, 2015.

[19] Y. Zhu, Z. Jia, Y. Yu, and X. Zeng, "Research on anti-corrosion property of rare earth inhibitor for X70 steel," *Journal of Rare Earths*, vol. 31, no. 7, pp. 734–740, 2013.

[20] S. Bernal, F. J. Botana, J. J. Calvino, M. Marcos, J. A. Perez-Omil, and H. Vidal, "Lanthanide salts as alternative corrosion inhibitors," *Journal of Alloys and Compounds*, vol. 225, no. 1-2, pp. 638–641, 1995.

[21] B. Davó and J. J. De Damborenea, "Use of rare earth salts as electrochemical corrosion inhibitors for an Al–Li–Cu (8090)

alloy in 3.56% NaCl," *Electrochimica Acta*, vol. 49, no. 27, pp. 4957–4965, 2004.

[22] D. Ho, N. Brack, J. Scully, T. Markley, M. Forsyth, and B. Hinton, "Cerium dibutylphosphate as a corrosion inhibitor for AA2024-T3 aluminum alloys," *Journal of the Electrochemical Society*, vol. 153, no. 9, pp. B392–B401, 2006.

[23] H. Allachi, F. Chaouket, and K. Draoui, "Protection against corrosion in marine environments of AA6060 aluminium alloy by cerium chlorides," *Journal of Alloys and Compounds*, vol. 491, no. 1-2, pp. 223–229, 2010.

[24] D. M. Martinez de la Escalera, J. J. Ramos-Hernandez, E. Porcayo-Palafox, J. Porcayo-Calderon, J. G. Gonzalez-Rodriguez, and L. Martinez-Gomez, "Effect of Nd^{3+} ion concentration on the corrosion resistance of API X70 steel in chloride-rich environments," *Advances in Materials Science and Engineering*, vol. 2018, Article ID 9328317, 15 pages, 2018.

[25] A. Olafsen and H. Fjellvåg, "Synthesis of rare earth oxide carbonates and thermal stability of $Nd_2O_2CO_3$ II," *Journal of Materials Chemistry*, vol. 9, no. 10, pp. 2697–2702, 1999.

[26] X.-B. Chen, T. Cain, J. R. Scully, and N. Birbilis, "Technical note: experimental survey of corrosion potentials for rare earth metals Ce, Er, Gd, La, and Nd as a function of pH and chloride concentration," *Corrosion*, vol. 70, no. 4, pp. 323–328, 2013.

[27] M. A. Arenas, A. Conde, and J. J. de Damborenea, "Cerium: a suitable green corrosion inhibitor for Tinplate," *Corrosion Science*, vol. 44, no. 3, pp. 511–520, 2002.

[28] M. A. Amin, M. A. Ahmed, H. A. Arida et al., "Monitoring corrosion and corrosion control of iron in HCl by non-ionic surfactants of the TRITON-X series—Part III. Immersion time effects and theoretical studies," *Corrosion Science*, vol. 53, no. 5, pp. 1895–1909, 2011.

[29] M. S. Al-Otaibi, A. M. Al-Mayouf, M. Khan, A. A. Mousa, S. A. Al-Mazroa, and H. Z. Alkhathlan, "Corrosion inhibitory action of some plant extracts on the corrosion of mild steel in acidic media," *Arabian Journal of Chemistry*, vol. 7, no. 3, pp. 340–346, 2014.

[30] J. Porcayo-Calderon, I. Regla, E. Vazquez-Velez, L. M. Martinez de la Escalera, J. Canto, and M. Casales-Diaz, "Effect of the unsaturation of the hydrocarbon chain of fatty-amides on the CO_2 corrosion of carbon steel using EIS and real-time corrosion measurement," *Journal of Spectroscopy*, vol. 2015, pp. 1–13, 2015.

[31] S. Godavarthi, J. Porcayo-Calderon, M. Casales-Diaz, E. Vazquez-Velez, A. Neri, and L. Martinez-Gomez, "Electrochemical analysis and quantum chemistry of Castor oil-based corrosion inhibitors," *Current Analytical Chemistry*, vol. 12, no. 5, pp. 476–488, 2016.

[32] J. Porcayo-Calderon, E. M. Rivera-Muñoz, C. Peza-Ledesma et al., "Sustainable development of palm oil: synthesis and electrochemical performance of corrosion inhibitors," *Journal of Electrochemical Science and Technology*, vol. 8, no. 2, pp. 133–145, 2017.

[33] K. A. Yasakau, M. L. Zheludkevich, S. V. Lamaka, and M. G. S. Ferreira, "Mechanism of corrosion inhibition of AA2024 by rare-earth compounds," *The Journal of Physical Chemistry B*, vol. 110, no. 11, pp. 5515–5528, 2006.

[34] E. A. Matter, S. Kozhukharov, M. Machkova, and V. Kozhukharov, "Comparison between the inhibition efficiencies of Ce(III) and Ce(IV) ammonium nitrates against corrosion of AA2024 aluminum alloy in solutions of low chloride concentration," *Corrosion Science*, vol. 62, pp. 22–33, 2012.

[35] T. Hu, H. Shi, T. Wei, F. Liu, S. Fan, and E.-H. Han, "Cerium tartrate as a corrosion inhibitor for AA 2024-T3," *Corrosion Science*, vol. 95, pp. 152–161, 2015.

[36] L. J. Zhang, Z. Zhang, J. Q. Zhang, and C. N. Cao, "The study of the $La(NO_3)_3$ inhibition on X70 pipeline steel in 3.0(wt.%) NaCl solution," *Materials and Corrosion*, vol. 56, no. 9, pp. 630–635, 2005.

[37] H. Ruiz-Luna, J. Porcayo-Calderon, J. M. Alvarado-Orozco et al., "Influence of oxidation treatments and surface finishing on the electrochemical behavior of Ni-20Cr HVOF coatings," *Journal of Materials Engineering and Performance*, vol. 26, no. 12, pp. 6064–6074, 2017.